Simulation of the Conformation and Dynamics of a Double-Helical Model for DNA

M. L. Huertas, S. Navarro, M. C. Lopez Martinez, and J. Garcia de la Torre

Departamento de Quimica Fisica, Universidad de Murcia, 30071 Murcia, Spain

ABSTRACT   We propose a partially flexible, double-helical model for describing the conformational and dynamic properties of DNA. In this model, each nucleotide is represented by one element (bead), and the known geometrical features of the double helix are incorporated in the equilibrium conformation. Each bead is connected to a few neighbor beads in both strands by means of stiff springs that maintain the connectivity but still allow for some extent of flexibility and internal motion. We have used Brownian dynamics simulation to sample the conformational space and monitor the overall and internal dynamics of short DNA pieces, with up to 20 basepairs. From Brownian trajectories, we calculate the dimensions of the helix and estimate its persistence length. We obtain translational diffusion coefficient and various rotational relaxation times, including both overall rotation and internal motion. Although we have not carried out a detailed parameterization of the model, the calculated properties agree rather well with experimental data available for those oligomers.

INTRODUCTION

The conformation and dynamics of double-helical DNA are ultimately determined by the chemical structure and the interatomic forces. The modern molecular dynamics simulation techniques (McCammon and Harvey, 1987) could be used, in principle, to predict DNA flexibility and dynamic behavior from models with atomic resolution. However, the length and time scales for bending and torsional, internal motions (in the orders of 10^2 Å and 10^{-9}–10^{-7} s) are far beyond the reach of conventional possibilities. In addition, these aspects are influenced by the solvent due to viscous friction (as it is regarded in those scales). The procedures to account for solvent effects, such as inclusion of a number of explicit solvent molecules in the system, or stochastic terms in the algorithm, adds further complications to the molecular dynamics approach.

With this point of view, it seems that the prediction of flexibility and internal dynamics of DNA from the double-helical structure may require the sacrifice of atomic resolution, and the use of Brownian dynamics simulation technique (Ermak and McCammon, 1978). The helical structure can be preserved in a model in which each residue is replaced by a single element, placed on a helix having the geometrical parameters known for the biopolymer. With some adequate representation of the interelement forces, the Brownian dynamics of such a model can be conveniently simulated. For helical polypeptides, this approach was pioneered by McCammon and coworkers (Lee et al., 1987;

Wade et al., 1993) and used in subsequent works (Rey and Skolnick, 1991; Schneller and Weaver, 1993).

In a preceding paper (García de la Torre et al., 1994a), we proposed a rigid, double-helical model for DNA, in which each nucleotide is represented by a frictional, spherical element (García de la Torre and Horta, 1976). The purpose was the calculation of overall hydrodynamic properties, concretely translational and rotational diffusion coefficients, of very short DNA pieces. The used procedure was the bead-model treatment for the hydrodynamics of rigid structures of arbitrary shape (García de la Torre and Bloomfield, 1981; García de la Torre, 1989; García de la Torre et al., 1994b). We found that the results for overall translation and rotation were in excellent agreement with recent measurements on oligonucleotides of as few as eight basepairs (Eimer and Pecora, 1991). This indicates that the hydrodynamics that is used in bead-model calculation, as well as in Brownian dynamics simulation, can be pushed down to molecular level. For the purpose of overall dynamics, the double-helical model was essentially rigid and, when necessary, internal motions were treated as corrections to the rigid-body behavior (Lipari and Szabo, 1982a, b; Schurr, 1984; Schurr and Fujimoto, 1988).

In the present work, we consider a double-helical model with some extent of flexibility, which makes it able to experience deformation and internal motions such as bending and torsions. Those motions are simulated from the very first principles of Brownian motion, using the Brownian dynamics simulation techniques. We anticipate that our mechanical model of the double helix is rather simple. Actually, we intended to use a minimal model that should describe the geometrical features of the helix and the essential internal motions, with only a few simple interactions. Our goal is to show that such a model is able to reproduce not only the qualitative aspects of the conformation and dynamics of the helix, but also to predict precisely various experimental data.

MODEL, SIMULATION, AND PROPERTIES

In our hydrodynamic model of DNA, each nucleotide is replaced by a spherical bead. (García de la Torre and Horta, 1976). The number of beads is $N = 2N_{bp}$, where N_{bp} is the number of basepairs. For simplicity, we assume that the four types of nucleotides have the same hydrodynamic radius, σ. The model is based on a "rigid" bead-model of the helix (García de la Torre et al., 1994a), which is now considered as the equilibrium conformation, and some extent of flexibility is introduced in a simplified manner by means of stiff, harmonic springs.

Equilibrium conformation

The equilibrium, or zero-energy, conformation is an undistorted double helix with straight helical axis (see Fig. 1). This conformation is the same as the rigid structure considered in our previous paper (García de la Torre et al., 1994a). The geometry of the helix is characterized by the pitch, P, and the radius A. If the helical axis is z, the parametric equations of the helix are

$$\left.\begin{array}{l} x^{eq} = A\cos(t + \phi) \\ y^{eq} = A\sin(t + \phi) \\ z^{eq} = Ht/2\pi \end{array}\right\} \quad (1)$$

The parameter t goes from $t = 0$ to $t = 2\pi n_t$, where n_t is the number of helical turns (not necessarily integer). One of the strands of the helix is described by Eq. 1 with $\phi = 180°$. If we take $\phi = \pi$ (180°) for the second strand, the resulting helix has binary symmetry around the z axis, and the structure looks unrealistic because the two helical grooves are identical. Taking a different value, say $\phi = 120°$, the aspect of the model is quite similar to that of B-DNA, exhibiting major and minor grooves.

In this equilibrium structure, spherical elements representing the nucleotides are placed on each of the two helices, with equal spacing and a density given by the number of residues per turn, n, in the DNA, so that $N_{bp} = nn_t$. It is easily found that the coordinates of the beads in the helical structure are given by Eq. 1 with

$$\left.\begin{array}{ll} t_i = 2\pi(i - 1)/n, & \phi = 180, \quad i = 1, 2, \ldots, N_{bp} \\ & \text{for strand 1} \\ t_i = 2\pi(i - N_{bp} - 1)/n, & \phi \le 180, \quad i = N_{bp} + 1, \ldots, 2N_{bp} \\ & \text{for strand 2} \end{array}\right\}$$

$$(2)$$

As discussed in our previous work, we choose the bead radius σ in such a way that neighbor beads in a strand, with center-to-center distance b, are touching (this is not reflected in Fig. 1). Thus, σ is determined by the other parameters of the helix (García de la Torre et al., 1994a) as $\sigma = b/2$ where $b = \{2A^2[1 - \cos(2\pi/n)] + (2\pi/n)^2\}^{1/2}$. For the numerical simulations, we have used the geometrical quantities proper of B-DNA: $H = 34$ Å, $n_t = 10$, and $A = 10$ Å. For this case, $b = 7.0$ Å and the bead radius is $\sigma = 3.5$ Å.

Flexibility

In the slightly flexible double helix we assume that, in a short-range scale, the motion of the elements in the model consists of small-amplitude displacements with respect to the equilibrium configuration described above. Accordingly, the distance r_{ij} between elements close within the structure (neighbors or next neighbors, either in the same strand or in the facing one), will fluctuate around the equilibrium value, $r_{ij}^{eq} = r_j^{eq} - r_i^{eq}$, where the position vectors r_j^{eq} in the equilibrium structure have the coordinates given
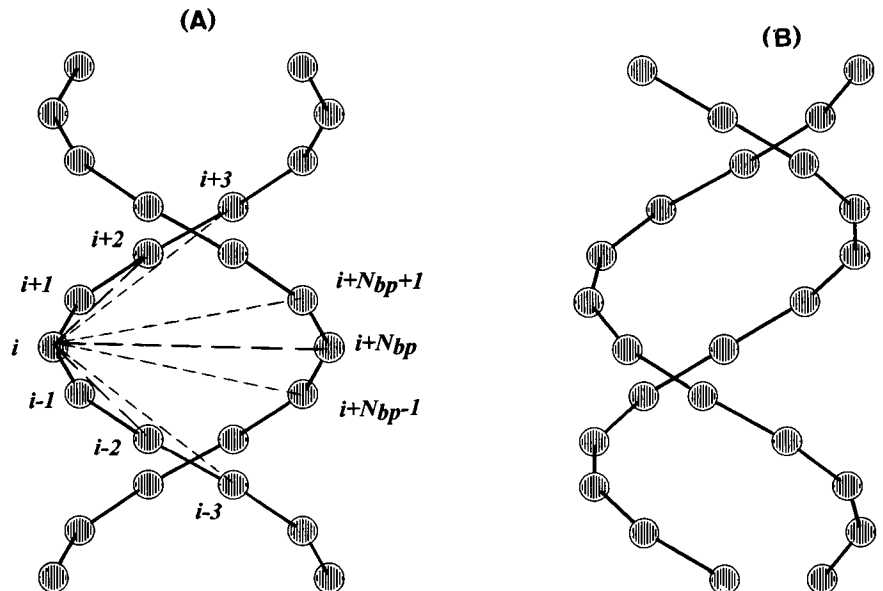

FIGURE 1 Double-helical structures (in the equilibrium, zero-energy conformation), showing the springs acting on any bead. The bead radius in the figure has been drawn smaller than in the real model for the sake of clarity (see also Fig. 1 of García de la Torre et al. (1994b). (A), symmetric helix, $\phi = 180°$. (B) asymmetric helix, $\phi = 120°$.

(A)

(B)

by Eq. 2. A very simple way to model this situation can be achieved assuming that beads i and j are joined by a stiff spring, which contributes to the potential energy of the molecule with

$$V_{ij} = k_{ij}(r_{ij} - r_{ij}^{eq})^2 \qquad (3)$$

In this work, we have tried to minimize the number of interactions that maintain the double-helical aspect of the structure and provide a sufficiently rigid structure at a short scale. We have found that this can be done if each bead i is linked to: 1) beads $i \pm 1$, i.e., first neighbors in the same strand, thus maintaining the connectivity, and keeping the instantaneous length of the virtual bonds close to b; 2) beads $i \pm 2$, i.e., second neighbors in the same strand, which somehow represent the bond angle interactions; 3) beads $i \pm 3$, i.e., third neighbors in the same strand, which somehow represent the torsional interactions; 4) bead $i + N_{bp}$ (or $i - N_{bp}$) in the opposite strand, representing the interaction between nucleotides forming basepairs; 5) beads $i + N_{bp} \pm 1$ (or $i - N_{bp} \pm 1$) between a bead in one strand and the first neighbors of its pair in the other strand. This interaction was necessary to keep the two strands interwound, and may be assigned to basepair stacking.

Thus, there are only five types of springs and every bead supports springs linking it with seven other beads; four in the same strand and three in the opposite one. (This has the obvious exception for the end or last-to-end beads in both strands.) The helical structure with the connecting springs is illustrated in Fig. 1.

The total force acting on bead i is given by

$$\mathbf{F}_i = 2 \sum_{j=1}^{N} k_{ij}(r_{ij} - r_{ij}^{eq})\mathbf{u}_{ij} \qquad (4)$$

where $\mathbf{u}_{ij} = \mathbf{r}_{ij}/r_{ij}$ is the unitary distance vector, and the total potential energy of the molecule is given by

$$V = \frac{1}{2} \sum_{i=1}^{N} \sum_{j=1}^{N} k_{ij}(r_{ij} - r_{ij}^{eq})^2 \qquad (5)$$

In Eqs. 4 and 5, the summation over j is restricted to the beads to which bead i is linked, as described above.

As commented in the Introduction, the present work is a preliminary study of the behavior of the flexible double-helical model. Therefore, we have not attempted a precise, quantitative parameterization of the model constants, i.e., the spring constants for the various types of springs. We have just empirically tried a few sets of parameters (the simulations are expensive, as noted below), finding that a simple set in which all the spring constants were identical, $k_{ij} = 100$ in units of kT/b^2 ($k_{ij} = 8.2$ dyn/cm) was able to predict quite well a number of experimental properties, as it will become apparent through the Results section.

Brownian dynamics simulation

The Brownian dynamics of the double helical model is simulated using a procedure based on the first-order algorithm of Ermak-McCammon (1978), with a modification proposed by Iniesta and García de la Torre (1990). Each step is taken twice, in a predictor-corrector manner, and the position of the beads $\mathbf{r}_i$ after the time step, Δt, are obtained from the previous ones, $\mathbf{r}_i^0$, according to

$$\mathbf{r}' = \mathbf{r}^0 + \frac{\Delta t}{kT}\mathbf{D}^0 \cdot \mathbf{F}^0 + \Delta t(\nabla_r \mathbf{D})^0 + \mathbf{R}^0 \qquad (6)$$

$$\mathbf{r} = \mathbf{r}^0 + \frac{\Delta t}{kT}\frac{1}{2}(\mathbf{D}^0 \cdot \mathbf{F}^0 + \mathbf{D}' \cdot \mathbf{F}')$$
$$+ \Delta t \frac{1}{2}[(\nabla_r \mathbf{D})' + (\nabla_r \mathbf{D})^0] + \mathbf{R}' \qquad (7)$$

Equation 6 is for the predictor substep, which is taken with basis on the quantities corresponding to the initial conformation, $\mathbf{r}^0$, denoted with the 0 superscript. In this step, an estimate, $\mathbf{r}'$, of the final conformation is obtained, and the necessary quantities are evaluated at it. Next the corrector step is taken as indicated in Eq. 7, again from the initial conformation, $\mathbf{r}^0$, but using quantities that are the mean of those at $\mathbf{r}^0$ and $\mathbf{r}'$. Although the step in our predictor-corrector procedure is equivalent to two Ermak-McCammon steps and subsequently it takes about twice the CPU time of the latter, longer time steps are allowed and there is a demonstrated increase in efficiency (Chirico and Langowski, 1992).

The $3N$ components of the vectors $\mathbf{r}$ and $\mathbf{F}$ are the coordinates, $\mathbf{r}_i$, and the mechanical forces $\mathbf{F}_i$ on the N beads, $\mathbf{D}$ is the $3N \times 3N$ diffusion supermatrix whose ij-blocks are the diffusion tensors, $\mathbf{D}_{ij}$. $\mathbf{R}^0$ and $\mathbf{R}'$ are random vectors with covariance matrix equal to $2\Delta t\mathbf{D}^0$ and $2\Delta t\mathbf{D}'$, respectively. They are calculated from Gaussianly distributed random vectors of zero mean and unit covariance, $\mathbf{q}$ and $\mathbf{q}'$, as $\mathbf{R}^0 = \sqrt{2\Delta t}\sigma^0\mathbf{q}$ or $\mathbf{R}' = \sqrt{2\Delta t}\sigma'\mathbf{q}'$, where the $3N \times 3N$ matrix σ is obtained from the square root of $\mathbf{D}$ (Allison and McCammon, 1984).

The ii blocks of the diffusion supermatrix are always given by $\mathbf{D}_{ii} = (kT/\zeta_i)\mathbf{I}$, where $\mathbf{I}$ is the unit 3×3 matrix, ζ_i is the friction coefficients of the bead, $\zeta_i = 6\pi\eta_0\sigma$, where η_0 is the viscosity of the solvent ($\eta_0 = 0.01$ for water at 20°C). For the simulation of dynamic properties, the hydrodynamic interaction (HI) between beads must be properly accounted for. We accomplish this using the Rotne-Prager-Yamakawa modification of the Oseen tensor, (Rotne and Prager, 1969; Yamakawa, 1970), which corrects for the non-pointlike nature of the frictional elements and describes correctly the possibility of overlapping (of equal-sized beads). Thus, we include HI setting $\mathbf{D}_{ij} = kT\mathbf{T}_{ij}$, where $\mathbf{T}_{ij}$ is the above-mentioned tensor.

Hydrodynamic interaction is neglected if we set $\mathbf{D}_{ij} = \mathbf{0}$ ($i \neq j$) in Eq. 6. Thus, the Iniesta-García de la Torre

algorithm (1990) simplifies to

$$\mathbf{r}_i' = \mathbf{r}_i^0 + \frac{\Delta t}{\zeta_i} \mathbf{F}_i^0 + \left(\frac{2\Delta t kT}{\zeta_i}\right)^{1/2} \mathbf{q}_i \qquad (8)$$

$$\mathbf{r}_i = \mathbf{r}_i^0 + \frac{\Delta t}{\zeta_i} \frac{1}{2} (\mathbf{F}_i^0 + \mathbf{F}_i') + \left(\frac{2\Delta t kT}{\zeta_i}\right)^{1/2} \mathbf{q}_i' \qquad (9)$$

This noHI algorithm requires much less CPU time than the full-HI procedure. The interest of this comes from the fact that equilibrium (nondynamic) properties can be simulated without HI, because they do not depend on the rate of dynamic processes. In other words, Brownian dynamics simulation without HI (noHI BD) can be used as an efficient procedure to sample the conformational variability of the molecule.

Regarding computing time, we note that, typically, every 10^4 steps of BD simulation of a model with $N = 12 + 12 = 24$ beads with HI requires ~ 220 s of CPU time in the MIPS R4400, 150 MHz of a SG Indigo2 workstation. In the same conditions, the BD simulation with noHI takes only 13 s. Furthermore, computer time grows as N^3 with HI, but without HI, it is just proportional to N.

The computational cost of Brownian dynamics simulation can be drastically reduced if the hydrodynamic interaction effect is not considered rigorously, being instead represented in an approximate way by an interaction tensor which is orientationally and conformationally preaveraged, as it was usual in early hydrodynamic theories (Yamakawa, 1971). This avoids the most time-consuming part of the algorithm, namely the calculation of matrix σ at every time step. However, it is known that the preaveraging approximation introduces some errors in the hydrodynamic properties of rigid and flexible molecules (García de la Torre et al., 1983, 1984, 1987). For instance, the rotational coefficient of a long, straight rod calculated with preaveraged HI presents a quite large error (García de la Torre et al., 1983). In the present work we aimed at the most accurate possible study of our double-helical model. Therefore, we decided not to make any hydrodynamic approximation that could be appreciably reflected in the final results, perhaps vitiating the comparison with experimental values. Anyhow, the possibility of speeding up the simulations with approximate hydrodynamics deserves further study.

RESULTS AND DISCUSSION

Equilibrium properties and conformations

The study of dynamic properties (simulation and comparison with experiments) to be presented later is restricted to short DNA fragments due to the high computational cost of BD with HI. However, as the BD-noHI simulation is much faster, the configurational study can be extended to longer fragments. Indeed, this is required if one wishes to determine an essential property of DNA, namely the bending flexibility, which is not perceptible if the DNA pieces are too short.

As a preliminary check of the model, from sufficiently long BD-noHI trajectories, we evaluated the averages of bead-to-bead distances for bead pairs joined by springs. We recall that every bead is linked to five other beads in the model. The resulting values were within 1% of the equilibrium values, which indicates that the model maintains the desired high local rigidity.

The mean square radius of gyration, $\langle s^2 \rangle$, and the mean squared end-to-end distance, $\langle r^2 \rangle$, are among the most important properties to express the overall conformation of macromolecules. From the BD-noHI simulations, we calculated these properties for moderately long DNA fragments. For the end-to-end distance we take for the end of the double helix the midpoint between the terminal pair of beads.

Obtaining meaningful averages requires running sufficiently long simulations and sufficiently small time steps, and these two conditions are somehow in conflict. Tests like that shown in Fig. 2 were carried out in order to determine proper working conditions. When the time step is short enough, the moving averages converge well to the equilibrium value. The simulated trajectory is divided into six subtrajectories of which the first one is discarded. We average individually over each subtrajectory, and the final result is expressed as the mean of the subtrajectory averages. Also, from their standard deviation we evaluate the standard error of the mean.

In Table 1 we present results for the mean square end-to-end distance, $\langle r^2 \rangle$, and radius of gyration, $\langle s^2 \rangle$, obtained by BD-noHI. For short DNAs, the dimensions of the present
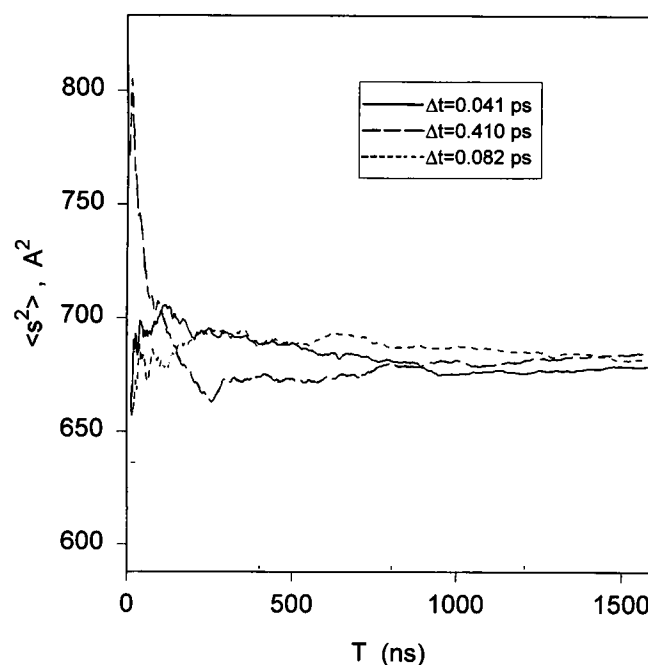

FIGURE 2 Running average for the mean square radius of gyration, $\langle s^2 \rangle$, for $N_{bp} = 24$, from BD-noHI trajectories, plotted versus trajectory duration, $T = n_{steps} \Delta t$.

TABLE 1   Values of $\langle r^2 \rangle$ and $\langle s^2 \rangle$ for double helices with varying length

N_{bp}	$\langle r^2 \rangle \times 10^{-3}$ Å^2		$\langle s^2 \rangle \times 10^{-3}$ Å^2	
	Flexible	Rigid	Flexible	Rigid
24	6.0 ± 0.3	6.1	0.70 ± 0.14	0.65
51	26 ± 2	29	2.58 ± 0.15	2.60
76	59 ± 2	65	5.52 ± 0.16	5.66
102	89 ± 14	116	8.9 ± 0.9	9.99
148	174 ± 16	249	17.1 ± 1.2	21.2

The results for the "perfect" rigid helix are also given.

model are very close to those for a "perfect" helix (a rigid structure with the equilibrium conformation). However, as the number of basepairs is increased, we note an increasing departure of the properties of the partially flexible model from those of the rigid one. Undoubtedly, that departure is a manifestation of the bending flexibility of the helix, which becomes more evident as the chain length increases. Also, for longer DNAs the contribution of the cross-section size and structure to the overall dimension, measured by $\langle s^2 \rangle$, becomes less important.

The overall conformation of double-helical DNA is customarily described by the wormlike chain model. For a wormlike filament of zero thickness, the mean square end-to-end distance is given by

$$\langle r^2 \rangle = 2PL\left[1 - \frac{P}{L} + \frac{P}{L}e^{-L/P}\right] \qquad (10)$$

where L is the contour length, which for B-DNA can be expressed as $L = (H/n_t)(N_{bp} - 1)$, or $L(\text{Å}) = 3.4(N_{bp} - 1)$, and P is the flexibility parameter, namely the persistence length, which for DNA takes the commonly accepted value $P \simeq 500$ Å. (See, for instance, García Molina et al., 1990). Equation 10 is applicable also to the distance between any two points within the filament, separated by contour distance L.

In order to compare our results with the wormlike chain, we make a previous reduction of the double helical structure to a linear filament. For any instantaneous conformation of the helix, we can obtain its instantaneous axis or "spine" as the line joining the midpoints of the bead pairs. Furthermore, we discard the terminal basepairs in order to avoid end effects. Particularly, we discard 10 basepairs at each end. Thus the end-to-end distance in the spine, r', is equivalent to the distance between basepairs numbered 11 and $N_{bp} - 10$, separated by $n_{bp} = N_{bp} - 20$, with an intervening contour length $L = 3.4(n_{bp} - 1) = 3.4(N_{bp} - 21)$. This is illustrated in Fig. 3.

The mean square $\langle r'^2 \rangle$ values obtained from our BD-noHI simulation for varying number of basepairs are plotted along with theoretical predictions of the wormlike model in Figure 4. For short DNAs, the persistence length cannot be analyzed because when $L \ll P$ the dimensions are independent of L. On the other hand, for longer fragments our results are compatible with a persistence length of ~ 500 Å,
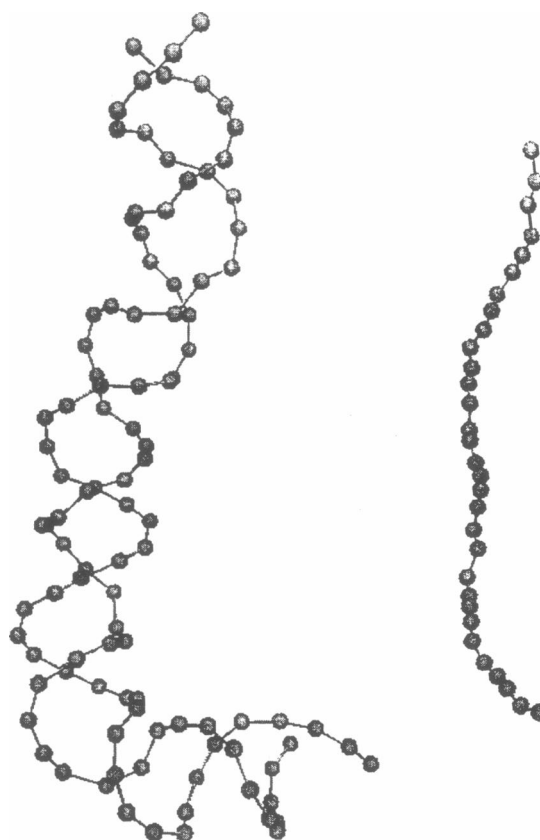

FIGURE 3   *Left*: Instantaneous conformation of a double helix with $N_{bp} = 51$, after a BD trajectory (no HI) of 160 ns. *Right*: The spine of the double helix after removal of 10 basepairs at each end.

or perhaps somehow larger. Our data point for $N_{bp} = 148$ ($n_{bp} = 128$) agrees very well with the value of the wormlike filament with $P = 500$ Å, although this can be somehow fortuitous due to the large error bar of our result.

Dynamic properties of short fragments: Translational diffusion

An essential aim of this work is the comparison of dynamic properties simulated for our model with experimental results available for DNA fragments of varying length. For the prediction of dynamic properties, the simulations must include hydrodynamic interaction (BD-HI), which makes the simulations much more expensive in terms of CPU time, as noted above. Thus, the simulations are necessarily restricted to oligonucleotides with few basepairs. Such is the case for the fragments for $N = 8$, 12, and 20 for which experimental data are available (Eimer et al., 1990; Birchall and Lane, 1990; Eimer and Pecora, 1991).

We carried out BD simulations with HI represented by the modified Oseen tensor. The time step was $\Delta t = 0.82 \times 10^{-4}$ ns $= 0.082$ ps, as in the noHI simulations. The trajectory lengths were 10^7, 2×10^7, and 4.5×10^7 steps (0.82, 1.64, and 3.69 μs) for $N_{bp} = 8$, 12, and 20. We wish to stress the difficulty of truly dynamic BD-HI simulation
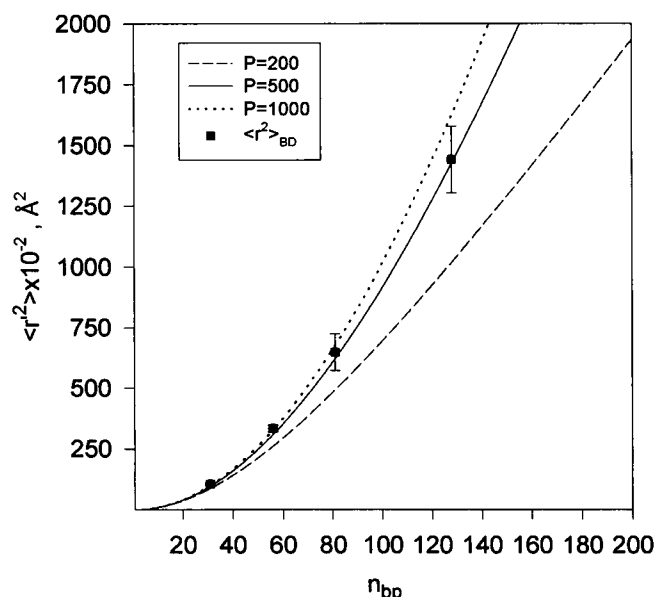
FIGURE 4 Mean square distance between two points of the *spine* of the helix separated by n_{bp} basepairs. Simulation results from BD-noHI are plotted along with theoretical predictions of the wormlike chain with the indicated values of the persistence length, P.

FIGURE 5 Center-of-mass correlation functions. The translational diffusion coefficient, D_t, is calculated from the slope of the straight lines. Results for $\phi = 120°$ and the three oligonucleotides.

for longer fragments: not only the CPU time grows very rapidly with N, but also longer trajectories must be generated since the rotational relaxation times also grows with N. (The trajectory for $N_{bp} = 20$ required ~1020 h of CPU in the above-described machine).

From the trajectories simulated by BD with HI, a variety of dynamic properties can be obtained by correlation analysis. One of the most simple but essential and experimentally accessible properties is the translational diffusion of the center-of-mass, D_t. This is obtained from the Einstein relationship for the correlation function of the displacement of the center of mass:

$$\langle [\mathbf{r}_{CM}(t) - \mathbf{r}_{CM}(0)]^2 \rangle = 6D_t t \qquad (11)$$

$\mathbf{r}_{CM}(0)$ is the position vector of the center of mass at some time, t_0, and $\mathbf{r}_{CM}(t)$ is the position after a time t has elapsed. The average $\langle \cdots \rangle$ is calculated over all the possible choices of the initial instant, t_0, along the simulated trajectory.

The correlation functions for the translational displacement (Eq. 11) are displayed in Fig. 5, where we appreciate the excellent linearity which allows a precise determination of the translational diffusion coefficients. The numerical results are given in Table 2. We note that the results for symmetric and asymmetric helices are very close to each other, and agree very well (within a small statistical uncertainty), with the experimental results of Eimer and Pecora (1991).

Rotational diffusion: End-over-end tumbling

For a nonrigid molecule, overall rotations cannot be clearly distinguished and separated from internal motion. One can
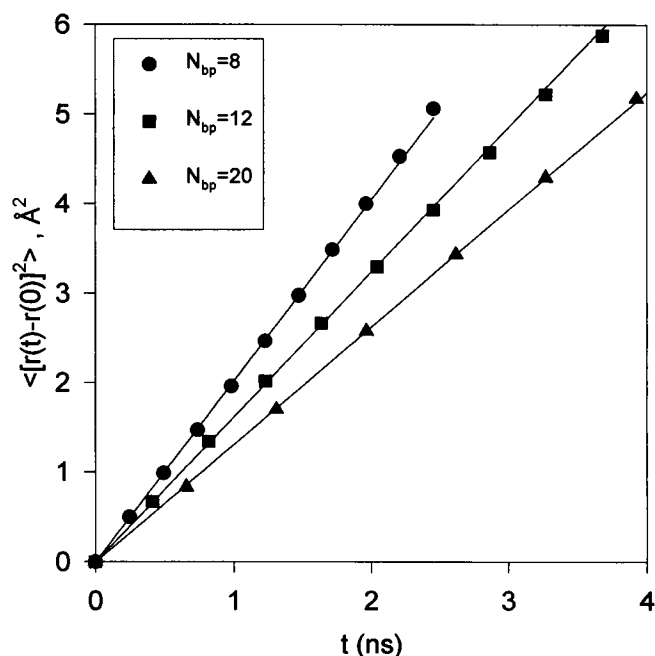
follow the Brownian rotational diffusion of a unitary vector **u** that is unambiguously defined for any arbitrary conformation of the particle. We can evaluate the function defined by

$$\langle P_2(t) \rangle_u = \langle (3 \cos^2\theta_u(t) - 1)/2 \rangle \qquad (12)$$

where $\cos\theta_u(t) = \mathbf{u}(t) \cdot \mathbf{u}(0)$. This function is the average (in the same sense as in Eq. 11) of the second Legendre polynomial of the angle traveled by vector **u** in a time interval t.

The calculated $\langle P_2(t) \rangle$ functions can be conveniently represented by a multiexponential decay, $\langle P_2(t) \rangle = a_1 e^{-t/\tau_1} + a_2 e^{-t/\tau_2} + \cdots$, with $a_1 + a_2 + \cdots = 1$. For these fits, we have employed the DISCRETE program of Provencher (1976a, 1976b). It is well known that the fit of data to a sum of exponentials is an ill-posed problem, regardless of the fitting procedure. Therefore we will not pay much attention to the individuals values of the amplitudes and relaxation

TABLE 2 Diffusion coefficients and relaxation times of the end-to-end vector of DNA oligonucleotides, obtained from BD simulation and compared with experimental data

N_{bp}	Simul. $\phi = 180°$	Simul. $\phi = 120°$	Exptl.
$D_t \times 10^7$ cm^{2}s^{-1}			
8	16.3 ± 1.8	16.7 ± 1.6	15.3
12	13.2 ± 0.4	13.4 ± 1.2	13.4
20	10.6 ± 0.3	10.8 ± 0.5	10.9
End-over-end τ_{ee} ns			
8	3.3 ± 0.2	3.9 ± 0.5	3.2
12	6.1 ± 0.7	7.8 ± 0.8	6.4
20	16.7 ± 1.7	19.0 ± 1.3	16.2

times, with the exception of the longest relaxation time, denoted as τ_1.

A mean relaxation time (sometimes called correlation time) can be defined as $\tau_{mean} = \int_0^\infty \langle P_2(t) \rangle dt$. Using the multiexponential fit as a mere function that represents the simulated $\langle P_2(t) \rangle$, the τ_{mean} can be calculated as

$$\tau_{mean} = a_1\tau_1 + a_2\tau_2 + \ldots \qquad (13)$$

We have experienced, in similar problems, that the parameter τ_{mean} is much more robust, (i.e., much less influenced by artifacts or fitting conditions, than the $a_i's$ and the $\tau_i's$ (García de la Torre, 1994; Carrasco et al., 1996).

One of the most immediate rotational problem is that when **u** is the end-to-end vector. In the case of a rigid structure (either the rod or the rigid double helix, the decay function $\langle P_2(t) \rangle_{ee}$ is a single exponential

$$\langle P_2(t) \rangle_{ee,rigid} = \exp(-6D_r^\perp t)$$

where $D_r^\perp$ is the rotational diffusion coefficient around an axis perpendicular to the rod or helix axis. There is a single relaxation time in this case, given by $\tau_{ee} = 1/(6D_r^\perp)$.

Experimentally, oligonucleotides with $N_{bp} = 8, 12$, and 20 are short enough so that their end-over-end tumbling can be monitored by depolarized dynamic light scattering (Eimer and Pecora, 1991), where a single-exponential decay of the pertinent correlation function is indeed observed.

In our simulations we also observe monoexponential decays for $\langle P_2(t) \rangle_{ee}$ (see Fig. 6), from which we have extracted the rotational relaxation times, τ_{ee}, which are listed
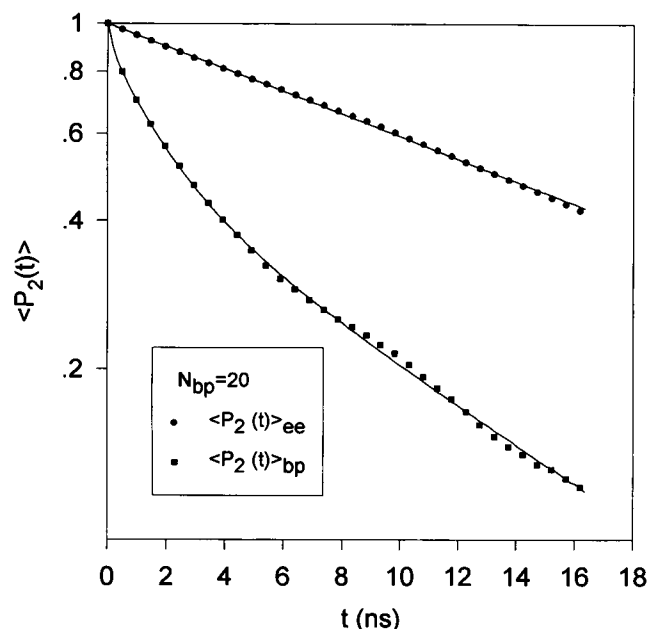

FIGURE 6 Semilog plot of the orientational correlation function, $\langle P_2(t) \rangle$ for two characteristic vectors: the end-to-end vector (*ee*) and the base-pair vector, perpendicular to the instantaneous axis of the helix (*bp*). The solid curves are the fitting functions, a single exponential in the first case and a double exponential in the latter.

and compared with the experimental data in Table 2. For this property we find an influence of the asymmetry of the helix that seems significant over the numerical error. We find that the result for the symmetric helix ($\phi = 180°$) agree very well with the experimental values, while the results for the asymmetric helix ($\phi = 120°$) deviate beyond their simulation uncertainty. We are not sure about where this situation comes from; it might be a computational artifact arising from cancellation of effects acting on opposite directions. As kindly pointed out by a referee, this may be related to the possibility that the water in the grooves of real DNA might be bound on a time scale comparable to rotational diffusion; a symmetric DNA could better represent the actual access of nonbound water to the grooves. At any rate, the global agreement between simulations and experiments is rather good.

Axial rotational diffusion and internal motion

Another relevant case of rotational diffusion is that corresponding to a vector associated to a basepair, pointing perpendicular to the helical axis. The dynamics of such a vector for a flexible helix contains an important contribution from internal torsional motion. The Brownian diffusion of this vector is monitored by time-resolved nuclear Overhauser effect cross-relaxation. This NMR technique has been applied recently to oligonucleotides (Eimer et al., 1990; Birchall and Lane, 1990). We simulate this rotational diffusion calculating, from the Brownian trajectories, the $\langle P_2(t) \rangle_{bp}$ function for the vector, $\mathbf{v_i}$, joining the two beads that represent a basepair, i and $i + N_{bp}$. For the rigid double helix (or rod), the theoretical result is

$$\langle P_2(t) \rangle_{bp} = \frac{1}{4}\exp(-6D_r^\perp t) + \frac{3}{4}\exp(-(4D_r^\perp + 2D_r^\parallel)t) \qquad (14)$$

where $D_r^\parallel$ is the rotational diffusion coefficient around the particle's main axis. Equation 14 is of the form of Eq. 13 with $a_1 = \frac{1}{4}$, $\tau_1 = 1/(6D_r^\perp)$, $a_2 = \frac{3}{4}$, $\tau_2 = 1/(4D_r^\perp + 2D_r^\parallel)$. The mean relaxation time is

$$\tau_{bp,rigid}^{mean} = \frac{1}{4}\frac{1}{(6D_r^\perp)} + \frac{3}{4}\frac{1}{(4D_r^\perp + 2D_r^\parallel)}$$

In our previous work (García de la Torre et al., 1994a) we calculated this quantity for the equilibrium conformation of the double helix using rigid-body hydrodynamics (García de la Torre et al., 1994b). Precisely, it was the deviation of calculated results from the NMR experimental data that indicated clearly the contribution to this property of the torsional, internal motions in the DNA double helix.

In Fig. 6 we display an example of a reorientational correlation function, $\langle P_2(t) \rangle_{bp}$, obtained from our BD trajectories. The fitting of $\langle P_2(t) \rangle_{bp}$ by DISCRETE gives rise to two or even three exponentials. As mentioned above, the most significant parameter is the mean correlation time τ_{bp}^{mean}, which is comparable to the experimental τ_{NMR}. We obtain τ_{bp}^{mean} from the coefficients of the fit using Eq. 13.

TABLE 3   Results from the correlation function for the basepair (perpendicular) vector

N_{bp}	a_1	τ_1 ns	τ_{bp}^{mean} ns	τ_{NMR} ns (exptl.)	$\tau_{bp, rigid}^{mean}$
8 (sym.)	0.72	3.13	2.56	1.5	3.2
8 (asym.)	0.94 ± 0.11	2.3 ± 0.3	2.2 ± 1.0		
12 (sym.)	0.80 ± 0.06	4.5 ± 0.8	3.8 ± 0.5	3.0	5.2
12 (asym.)	0.78 ± 0.16	4.4 ± 1.0	3.6 ± 1.0		
20 (sym.)	0.60 ± 0.03	9.5 ± 2.6	6.8 ± 1.2	5.7	10.6
20 (asym.)	0.50 ± 0.12	11.0 ± 2.6	6.3 ± 0.6		

The resulting values are presented in Table 3, where we have also included the lowest relaxation time and its amplitude, along with the value calculated for a rigid double helix in our previous work (García de la Torre et al., 1994a).

In Figure 7 we present our simulation results along with the experimental data and the prediction from the rigid double-helical model. Actually, we note again small differences between the $\phi = 180°$ and $\phi = 120°$ cases. The analysis of τ_{NMR} evidences the important improvement of the flexible model over the rigid one. The present simulation results are much closer to the experimental values than the former ones.

In our previous work, (García de la Torre et al., 1994a), the torsional, internal motion of the helix was applied a posteriori, superimposing treatments like the model-free approach of Lipari and Szabo (1982) or the treatment of Schurr and Fujimoto (1988) on the dynamics (studied a priori) of the rigid helix. In the present work, flexibility and internal motion are embodied in the model from its initial
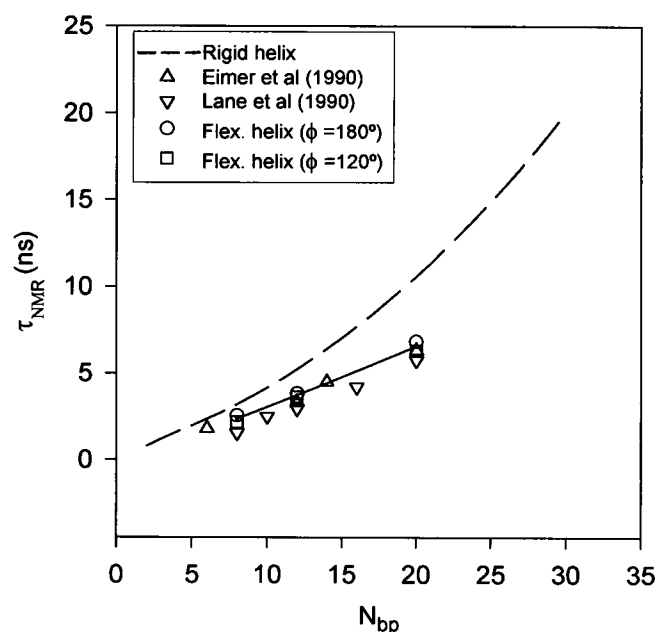

FIGURE 7   NMR NOE cross-relaxation times of DNA oligomers of up to 20 basepairs. Experimental data are from Eimer et al. (1990) and Lane et al. (1990). The dashed curve represents our former calculations for the rigid double-helical model (García de la Torre et al., 1994a). Our simulation results for N_{bp} = 8, 12, and 20 are also included; the solid line is just intended to guide the eye through them.
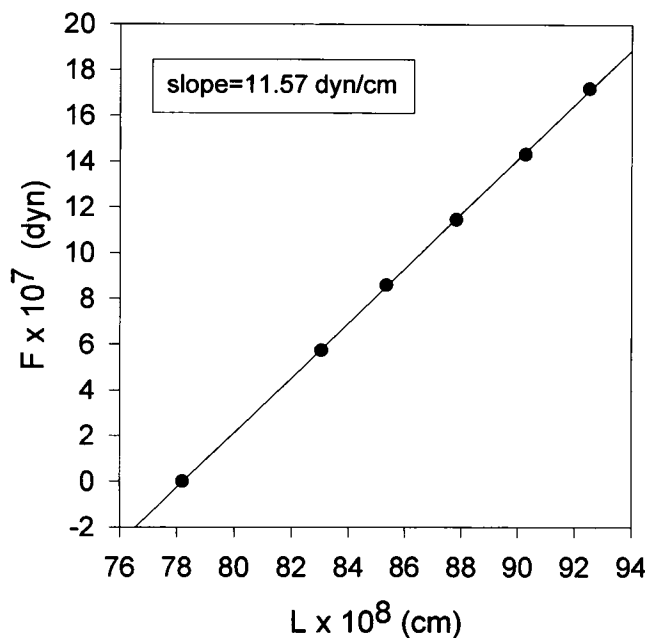
construction; indeed, the very same model is consistently used for all the properties.

Internal motions and rigidities

In the preceding subsections we have shown how our double-helical model is able to describe properly the dynamic properties that are more directly available from experiments. These properties, and particularly τ_{NMR}, contain mixed contributions from overall (rigid-body) motions and internal motions. After these calculations, and following suggestions of the referees of this paper, we carried out further analysis trying to characterize more specifically the internal motions and the associated rigidities.

For the determination of the stretching elasticity of our double-helical model, we found it possible and useful to employ a straightforward procedure based on our own Brownian dynamics algorithms. Starting from the straight, unstretched, equilibrium conformation, forces $+F$ and $-F$ were applied at both ends (actually, we applied $F/2$ to each bead in each terminal pair of beads). The final conformation under the action of the force was clearly obtained after a dynamics run in which the Brownian motion was switched off setting $q_i = q_i' = 0$ in Eqs. 8 and 9. In the stretched conformation, the helix is still straight but has a length L, measured along the z axis, greater than the equilibrium value, $L_0 = (N_{bp} - 1)H/n_t$. This is done for different values of the applied force, and the results are analyzed in terms of an elastic law $F = YS(L - L_0)/L_0$, where S is the cross-sectional area of DNA, taken as $S = \pi A^2$, and Y is the Young's modulus.

Figure 8 shows a typical result of the stretching simulations, displaying the linear dependence of F on L. From the slope, the Young's modulus of our model turns out to be $Y = 2.9 \times 10^8$ dyn/cm^2. In a very recent experiment, Smith et al. (1986) reported a modulus of 3.5×10^8 dyn/cm^2. The excellent agreement may be somehow fortuitous, since we did not make a detailed parameterization of the spring constants, which were rather assigned ad hoc values. Thanks to the simplicity of the procedure, we have also been able to study which of the various spring types contribute more to the stretching elasticity. For each spring type, the constant was doubled and halved, with the constants for the other springs remaining fixed at $100kT/b^2$. The results are displayed in Table 4, and show that the Young's modulus is most sensitive to the intrastrand springs. It seems clear that,

FIGURE 8 Stretching force versus elongation, L, for a double-helix with $N_{bp} = 24$, and all the spring constants set to $100\ kT/b^2$. The intercept at the horizontal axis is L_0, and the slope is equal to $\pi A^2 Y$.

if the spring constants are treated as adjustable parameters, the model might reproduce exactly the experimental Young's modulus.

Another type of relevant internal motion is the torsion of the double helix, manifested by local angular fluctuations of the mutual orientations of neighboring basepairs. We attempted a purely mechanic evaluation of the torsional stiffness, similar to that used above for stretching but applying torques at the terminal pairs of beads. Unfortunately, the convergence to a final structure was much slower and unstable, and therefore we gave up this procedure. Rather, we tried to obtain this information from the simulated Brownian trajectories.

As kindly noted to us by a referee, Fig. 6 does not show a sharp relaxation of local angular motions. According to

TABLE 4 Young's modulus of the double-helical bead-and-spring model

Spring	Force constant (kT/b^2 units)	$Y \times 10^{-8}$ dyn/cm²
All	100	2.89
$i \ldots i \pm 1$	50	2.74
	200	2.99
$i \ldots i \pm 2$	50	2.56
	200	3.15
$i \ldots i \pm 3$	50	2.47
	200	3.37
$i \ldots i \pm N_{bp}$	50	2.22
	200	3.57
$i \ldots i \pm N_{bp} \pm 1$	50	2.58
	200	3.18
Experimental		3.46

All the spring constants, except when specified, are set to $100kT/b^2$.

experimental studies of the amplitude of such motions (Eimer et al., 1990; Nuutero et al., 1994), $\langle P_2(t)\rangle_{bp}$ could decay down to ~0.8 in a very short time, of ~0.1 ns (Magde et al., 1983). In order to elucidate the amplitude and dynamics of the local angular motions, we tried to make a further analysis of the angle, β_i, subtended by consecutive basepair vectors $\mathbf{v}_i$ and $\mathbf{v}_{i+1}$. These angles are 36° in the undistorted, equilibrium conformation. We take $i = N_{bp}/2$, so that $\mathbf{v}_i$ and $\mathbf{v}_{i+1}$ are the innermost pair of vectors, thus minimizing end effects. The time-course described by θ_i along a Brownian trajectory is shown in Fig. 9. From this trace, we obtain an average value $\langle\beta\rangle = 34.0°$, while the r.m.s. fluctuation, $\delta\beta = (\langle\beta^2\rangle - \langle\beta\rangle^2)^{1/2}$, is estimated to be ~5.3°.

There has been some controversy in the literature concerning the amplitude of this fluctuation. For the amplitude of the orientational fluctuation of a vector rigidly attached to the basepair, Eimer et al. (1990) reported results leading to $\delta\theta = \langle\theta^2\rangle^{1/2}$ of up to 25°, while Nuutero et al. (1994), from a re-analysis of the data of Eimer et al. and from other studies, lower considerably the fluctuation, down to ~10°. Our $\delta\beta$, in which the fluctuation of two vectors are accumulated, is nearly equivalent to $\delta\theta$ (quite close although slightly larger than it). The result from our model, with all the spring constants set to $100kT/b^2$, $\delta\beta \approx 5.3°$, is even smaller than the smallest estimates from experimental studies. This finding does not throw any light into the abovementioned controversy, since it is the a posteriori result of a quite arbitrary choice of the spring constants that, as shown by this comparison, results in a too low value for the amplitude, thus probably overestimating the torsional rigidity of DNA. As in the case of the stretching elasticity, further refinements in this regard are left for future work.

Still regarding the local angular motion, we have made an analysis of its dynamics from the autocorrelation function $\langle\beta(t)\beta(0)\rangle$. An example is shown in Fig. 10. The decay curve is approximately described by a double exponential, with a fast relaxation time of ~0.04 ns and a slow one of ~0.54 ns. The mean relaxation time is 0.24 ns. This results are in acceptable agreement with the estimate of Magde et al. (1983) of ~0.1 ns for the relaxation of the local angular motions.

Finally, the third essential type of internal rigidity is that associated to bending. This is clearly manifested by the fluctuation in overall size, and characterized in terms of the persistence length. As these aspects have been well described in the first part of this work, we have not felt the need of a further study of bending at a local level.

CONCLUSIONS

The conformation and dynamics of the double-helical DNA can be described and simulated in terms of a simple model that embodies the structural features of the double helix and is yet able to predict long-scale properties. Modeling at the level of the repeating unit (one element per nucleotide), dynamic simulations of DNA can reach the time scale of
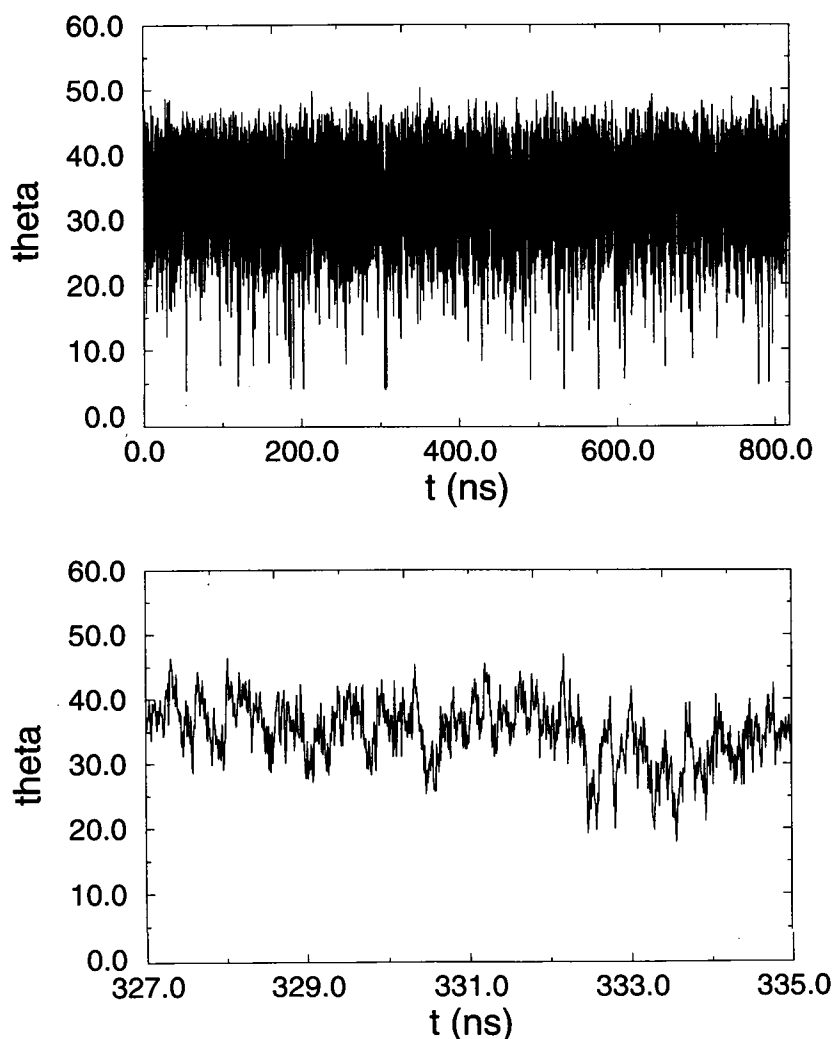
FIGURE 9   *(Top)* Fluctuation of the angle β_i during a long Brownian trajectory. *(Bottom)* Short-time detail, showing how fast the fluctuation is. Results are for $N_{bp} = 12$.

microseconds. By using Brownian dynamic simulation we have predicted a variety of properties of double-helical DNA, whose agreement with existing experimental data was quite satisfactory, and very good in some cases.

Translational diffusion coefficients and end-over-end rotational relaxation times of DNA oligomers with up to 20 basepairs agreed rather well with experimental data (Eimer et al., 1990), which indicates that the model possesses and maintains during its dynamics the correct size and shape of the real DNA piece.

The model also possesses an adequate flexibility. The bending flexibility is detected from the departure of the end-to-end distance and radius of gyration from the values for a straight, rigid helix. The amount of bending of our model is compatible with the wormlike chain description, with the customarily accepted persistence length of ~500 Å.

The motion manifested by the reorientational dynamics of a basepair vector perpendicular to the helical axis is a complex superposition of overall rotation, bending, and torsion. Experimentally, this reorientation corresponds to the NMR-NOE cross-relaxation of a pair of protons within the basepair (Eimer et al., 1990). While the rigid double

helix (García de la Torre et al., 1994a) had failed the prediction of the experimental relaxation times, our present simulation results for the corresponding relaxation time are quite close to the experimental values. This suggests that our flexible, double-helical model has an adequate torsional flexibility.

The hydrodynamics of DNA has been customarily described in terms of a straight string (for short fragments) or a wormlike chain (Bloomfield et al., 1974). In this representation, the details of the double-helical structure are neglected, being instead replaced by an effective, hydrated diameter. Actually, the hydrated diameter representation has been successfully used in most studies to date, describing adequately aspects related to the overall dynamics, in both Monte Carlo (Hagerman and Zimm, 1982; García Molina et al., 1990) and Brownian dynamics simulation (Allison, 1986; Allison et al., 1990; Heath et al., 1995). The advantages of our double-helical model (whose obvious disadvantage is simply computational cost) over the hydrated-diameter cylinder or worm are best noticed when one treats dynamics aspects involving, at least partially, internal motions. The present model allows for a more detailed descrip-
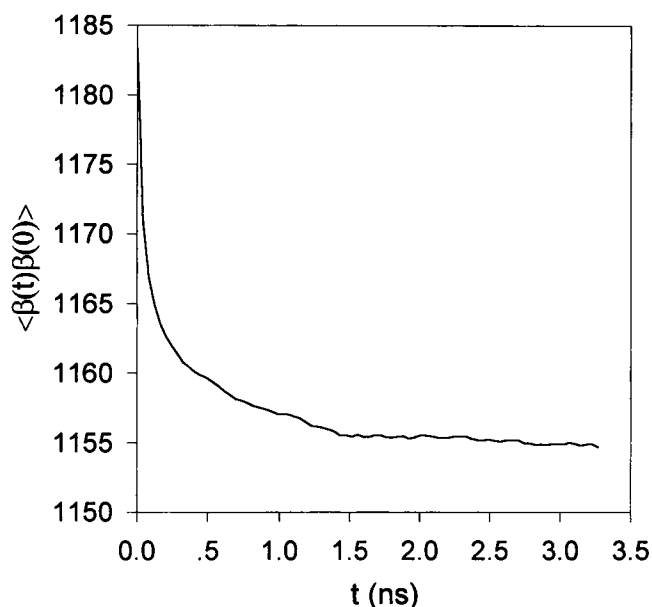
FIGURE 10   Autocorrelation function $\langle \beta(t)\beta(0) \rangle$ for $N_{bp} = 12$, which decays from $\langle \beta^2 \rangle$ to $\langle \beta \rangle^2$.

tion of local motions and rigidities in terms of parameters of a helical structure. One could even envision some special but very relevant problems, such as sequence-dependent dynamics, effects of nicks, and chain fracture, always in terms of the double-helical geometry of DNA.

REFERENCES

Allison, S. 1986. Brownian dynamics simulation of wrokmlike chains. Fluorescence depolarization and depolarized light scattering. *Macromolecules.* 19:118–124.

Allison, S., and J. McCammon. 1984. Transport properties of rigid and flexible macromolecules by Brownian dynamics simulation. *Biopolymers.* 23:167–187.

Allison, S., S. Sorlie, and R. Pecora. 1990. Brownian dynamics simulation of wormlike chains. Dynamic light scattering from a 2311 base pair DNA fragment. *Macromolecules.* 23:1110–1118.

Birchall, A. and A. Lane. 1990. Anisotropic rotation in nucleic acid fragments: significance for determination of structures from NMR data. *Eur. Biophys. J.* 19:73–78.

Bloomfield, V., D. Crothers, and I. Tinoco, Jr., editors. 1974. Physical Chemistry of Nucleic Acids. Harper & Row Publishing Co., New York.

Carrasco, B., A. Pérez Belmonte, M. López Martínez, and J. García de la Torre. 1996. Transient orientation and electrooptical properties of axially symmetric macromolecules in an electric field of arbitrary strength. *J. Chem. Phys.* 100:9900–9905.

Chirico, G. and J. Langowski. 1992. Calculating the hydrodynamic properties of DNA through a second-order Brownian dynamics algorithm. *Macromolecules.* 25:769–775.

Eimer, W. and R. Pecora. 1991. Rotational and translational diffusion of short rodlike molecules in solution: oligonucleotides. *J. Chem. Phys.* 94:2324–2329.

Eimer, W., J. Williamson, S. Boxer, and R. Pecora. 1990. Characterization of the overall and internal dynamics of short oligonucleotides by depolarized dynamic light scattering and NMR relaxation measurements. *Biochemistry.* 29:799–811.

Ermak, D. and J. McCammon. 1978. Brownian dynamics with hydrodynamic interactions. *J. Chem. Phys.* 69:1352–1360.

García de la Torre, J. 1989. Hydrodynamic properties of macromolecular assemblies. In Dynamic Properties of Macromolecular Assemblies. S. E. Harding, editor. The Royal Society of Chemistry, Cambridge, 3–31.

García de la Torre, J. 1994. Dynamics of segmentally flexible biological macromolecules. *Eur. Biophys. J.* 23:307–322.

García de la Torre, J., and V. Bloomfield. 1981. Hydrodynamic properties of complex, rigid, biological macromolecules. Theory and applications. *Q. Rev. Biophys.* 14:81–139.

García de la Torre, J. and A. Horta. 1976. Sedimentation coefficient and X-ray scattering of double helical model for DNA. *J. Chem. Phys.* 80:2028–2035.

García de la Torre, J., M. López Martínez, M. Tirado, and J. Freire. 1983. Approximate methods for calculating hydrodynamic properties of macromolecules in dilute solution. Theory and application to rigid structures. *Macromolecules.* 16:1121–1127.

García de la Torre, J., M. López Martínez, M. Tirado, and J. Freire. 1984. Monte Carlo study of hydrodynamic properties of flexible linear chains. Analysis of several approximate methods. *Macromolecules.* 17: 2715–2722.

García de la Torre, J., M. C. López Martínez, and J. García Molina. 1987. Approximate methods for calculating rotational diffusion constants of rigid macromolecules. *Macromolecules.* 20:661.

García de la Torre, J., S. Navarro, M. López Martínez, F. Diaz, and J. López Cascales. 1994a. HYDRO: a computer software for the prediction of hydrodynamic properties of macromolecules. *Biophys. J.* 67: 530–531.

García de la Torre, J., S. Navarro, and M. C. López Martínez. 1994b. Hydrodynamic properties of a double-helical model for DNA. *Biophys. J.* 66:1573–1579.

García Molina, J., M. C. López Martínez, and J. García de la Torre. 1990. Computer simulation of hydrodynamic properties of semiflexible macromolecules. Randomly broken chains, wormlike chains and analysis of properties of DNA. *Biopolymers.* 29:883–900.

Hagerman, P., and B. Zimm. 1982. Monte Carlo approach to the analysis of the rotational diffusion of wormlike chains. *Biopolymers.* 20: 1481–1502.

Heath, P., S. Allison, J. Gebe, and J. Schurr. 1995. A theory for electric dichroism and birefringence decays and depolarized dynamic light scattering of weakly bending rods. *Macromolecules.* 28:6600–6607.

Iniesta, A., and J. Garcia de la Torre. 1990. A second order algorith for the simulation of the Brownian dynamics of macromolecular models. *J. Chem. Phys.* 92:2015–2019.

Lee, S., M. Karplus, D. Bashford, and D. Weaver. 1987. Brownian dynamics simulation of protein folding: A study of the diffusion-collision model. *Biopolymers.* 26:481–506.

Lipari and Szabo, A. 1982a. Model-free approach to the interpretation of nuclear magnetic resonance relaxation in macromolecules. 1. Theory and range of validity. *J. Am. Chem. Soc.* 104:4546–4559.

Lipari and Szabo, A. 1982b. Model-free approach to the interpretation of nuclear magnetic resonance relaxation in macromolecules. 2. Analysis of experimental result. *J. Am. Chem. Soc.* 104:4559–4570.

Magde, D., M. Zappala, W. Knox, and T. Norlund. 1983. Picosecond fluorescence anisotropy decay in the ethidium-DNA complex. *J. Phys. Chem.* 87:3286–3296.

McCammon, J., and S. Harvey, editors. 1987. Dynamics of Proteins and Nucleic Acids. Cambridge University Press, Cambridge.

Nuutero, S., B. Fujimoto, P. Flynn, R. Reid, N. Ribeiro, and J. Schurr. 1994. The amplitude of local angular motions of purines in DNA in solution. *Biopolymers.* 34:463–480.

Provencher, S. 1976a. An eigenfunction expansion method for the analysis of exponential decay curves. *J. Chem. Phys.* 64:2772–2777.

Provencher, S. 1976b. A Fourier method for the analysis of exponential decay curves. *Biophys. J.* 16:151–170.

Rey, A. and V. Skolnick. 1991. Comparison of lattice Monte Carlo and Brownian dynamics folding pathways of α-helical hairpins. *Chem. Phys.* 158:199–219.

Rotne, J. and S. Prager. 1969. Variational treatment of hydrodynamic interaction in polymers. *J. Chem. Phys.* 50:4831–4837.

Schneller, W. and D. Weaver. 1993. Simulation of α-helix to coil transitions in simplified polyvaline: equilibrium properties and Brownian dynamics. *Biopolymers.* 33:1519–1535.

Schurr, J. 1984. Rotational diffusion of deformable macromolecules with mean local cylindrical symmetry. *J. Chem. Phys.* 84:71–96.

Schurr, J. and B. Fujimoto. 1988. The amplitude of local angular motions of intercalated dyes and bases in DNA. *Biopolymers.* 27:1543–1569.

Smith, S., Y. Cui, and C. Burtamante. 1986. Overstretching B-DNA: the elastic response of individual double-stranded and single-stranded DNA molecules. *Science.* 271:795–799.

Wade, R., M. Davis, B. Luty, J. Madura, and J. McCammon. 1993. Gating of the active site of triose phosphate isomerase: Brownian dynamics simulation of flexible peptide loops in the enzyme. *Biophys. J.* 64:9–15.

Yamakawa, H. 1970. Transport properties of polymer chains in dilute solution: Hydrodynamic interaction. *J. Chem. Phys.* 53:436–443.

Yamakawa, H., editor 1971. Modern Theory of Polymer Solutions. Harper & Row Publishing Co., New York.